

# The “Third Body” Approach to Joining of Metals by Simple Shear under Pressure

Yan Beygelzimer, Karl C. Grötzinger, Mathias Liewald, Yuri Estrin, and Roman Kulagin\*

A continuum mechanics approach to cold welding (CW) of metals under shear is considered. The main idea is to treat a weld joint as an extra material—a “third body” in its own right. Its properties stem from plastic co-deformation of the two contacting alloys. The mechanical characteristics of the weld joint, i.e., its strength and plasticity in the complex stress state, are determined by the deformation history of the “third body.” The proposed approach enables a unified description of the CW process itself, as well as the subsequent variation of shape of the composite material with the weld joint.

## 1. Introduction

Compared to other plastic deformation modes, simple shear is characterized by certain specific features.<sup>[1]</sup> They manifest themselves in the group properties of the geometric transformation associated with simple shear and in the effect it has on materials.<sup>[2–4]</sup> This is why simple shear, which is intrinsic in processes such as high-pressure torsion,<sup>[5–7]</sup> equal channel angular pressing,<sup>[8]</sup> and twist extrusion,<sup>[9]</sup> is widely used to form ultrafine-grained structures in metals and alloys and to create new

materials by processing powders or layered materials.<sup>[10]</sup> In the latter case, the desired results are achieved owing to enhancement of diffusion and convective mass transfer through plastic deformation by simple shear.<sup>[11–13]</sup> This enhancement leads to active mixing of the constituent components and the induction of physicochemical transformations in the deforming sample. Similarly, simple shear induces joining of metals and the formation of new phases in the contact zone under dry friction and wear conditions.<sup>[14–16]</sup> An

interesting application could be the production of various alloys by processing elemental powders using the high-pressure torsion (HPT) method.<sup>[17–19]</sup> The seminal work of the research group of Reinhard Pippan on the use of HPT,<sup>[20,21]</sup> and, notably, their studies on what can be called mechanical synthesis of powders for creating new materials,<sup>[22,23]</sup> is a strong motivation for developing modeling approaches to their experimental findings.

Mathematical modeling of processes occurring when metals are joined by simple shear is greatly complicated by the pluridisciplinary nature of the phenomenon. We believe that the concept of a “third body”, which has been developed in works on friction and wear, can provide a useful modeling tool.<sup>[24–26]</sup> The “third body” (TBody) associated with the contact zone is regarded as a separate entity, which includes rough surfaces, thin surface layers of the materials engaged in shear, as well as films, lubricants, contaminants, gases, and wear products, located on the surfaces in contact and in the pores entrapped by them. In this concept, friction at the boundary between the two bodies is associated with the shear resistance of the TBody. Singling out the contact zone as a separate object makes it possible to address the mentioned pluridisciplinary problems.<sup>[24]</sup>

We see the TBody approach as a practical vehicle to constructing mathematical models of metal joining that account for the formation of the structure and properties of a TBody during its plastic deformation under pressure. There are several TBody-based models devised for research in friction and wear.<sup>[25–29]</sup> They make it possible to analyze the processes occurring in the friction zone, identify characteristic patterns in the genesis of the friction force, and find its dependence on external factors, including pressure, sliding speed, and temperature. That is why we adopt the promising TBody approach in the present work.

It should be mentioned that further methods similar in spirit to the TBody concept have been put forward in the past. Specifically, the cohesive zone models should be referred to as

Y. Beygelzimer

Donetsk Institute for Physics and Engineering named after A.A. Galkin  
National Academy of Sciences of Ukraine  
Nauki Avenue, 46, 03028 Kyiv, Ukraine

K. C. Grötzinger, M. Liewald

Institute for Metal Forming Technology  
University of Stuttgart  
Holzgartenstr. 17, 70174 Stuttgart, Germany

Y. Estrin

Department of Materials Science and Engineering  
Monash University  
22 Alliance Lane, Clayton 3800, Australia

R. Kulagin

Institute of Nanotechnology  
Karlsruhe Institute of Technology  
Hermann-von-Helmholtz-Platz 1, 76344 Eggenstein-Leopoldshafen,  
Germany  
E-mail: roman.kulagin@kit.edu

 The ORCID identification number(s) for the author(s) of this article can be found under <https://doi.org/10.1002/adem.202400388>.

© 2024 The Authors. Advanced Engineering Materials published by Wiley-VCH GmbH. This is an open access article under the terms of the Creative Commons Attribution-NonCommercial License, which permits use, distribution and reproduction in any medium, provided the original work is properly cited and is not used for commercial purposes.

DOI: 10.1002/adem.202400388

being cognate with the TBody ones.<sup>[30,31]</sup> Another group of models focus on the thermal effects in frictional sliding and connecting the thermomechanical behavior of the bulk material with the local processes of asperity shearing within a near surface layer.<sup>[32–34]</sup> We mention these models here as in some ways the asperity shear-affected near-surface layer introduced there is akin to a “third body” of interest.

In the present article, we pose the problem of describing metal joining under simple shear in terms of the “third body” concept, propose and analyze a continuum model for a TBody, and illustrate the efficacy of the approach by way of example. According to the model proposed, failure of the bond occurs when irreversible deformation of the TBody sets in. The strength of the bond in a given stress state is determined by the yield locus of the TBody in the stress space. Notably, this approach allows solving coupled problems. Indeed, it takes into account the influence of the mechanical properties of the bond created by plastic deformation on the character of the plastic flow of the composite structure in which it has been formed in the first place. The article introduces an experimental approach and methodology for bonding metals through shear under pressure. This method is proposed to elucidate the parameters associated with the TBody model.

## 2. Posing the Problem

Figure 1a shows the schematics of a contact zone between two solid bodies, which in a continuum approach is represented by a thin layer of some “equivalent” material—a “third body” introduced above (Figure 1b). Equivalence, in this case, means that in terms of deformation and failure, the TBody imitates the behavior of the real contact zone, namely: (i) the rheology of the TBody describes the relation between the stresses in the bond and the deformation of the composite, defined by the relative displacement of its constituents and (ii) the limit state of the TBody corresponds to the failure of the bond. Henceforth, the limit state of a TBody is associated with the onset of plastic flow therein.

The TBody includes thin surface layers involved in shear deformation. Their thickness is of the order of the height of the surface roughness peaks,  $h \sim (R_{z1} + R_{z2})$ , where  $h$  is the thickness of the TBody, and  $R_{z1}$  and  $R_{z2}$  denote the average height of the peaks (asperities) associated with the surface roughness of the respective metal.

The main assumptions we are going to make in this article when constructing a continuum TBody model are summarized later. They are not inherent to the approach and are used just to enable an illustration of some of the capabilities of the model as exemplified by the model thus specified.

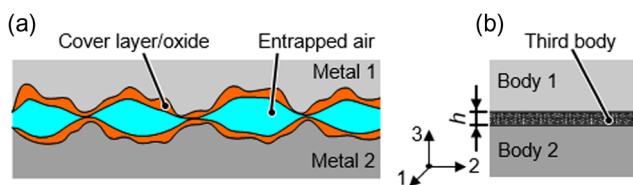


**Figure 1.** Posing the problem for the exemplary case of cold welding based on the TBody concept: a) sketch of the contact zone between two metals and b) schematics of the TBody approach.

Considered as a continuum, the TBody is characterized by a stress–strain state, which, following the mathematical theory of plasticity,<sup>[35]</sup> is described by the stress tensor  $\sigma_{ij}$  and the strain rate tensor  $\dot{\epsilon}_{ij}(i, j = 1, 2, 3)$ . We further assume that the TBody is an isotropic material. Certainly, this is a strong assumption, but even under this restrictive condition, interesting and useful results can be obtained. This is suggested by the success of applying the classical plasticity theory to calculations of various processes of cold forming of metals under pressure. In these processes, the material is either anisotropic initially or acquires anisotropy as a result of deformation. While the plasticity theory disregards this factor, it still provides a qualitatively correct description of many forming processes and even yields quantitative estimates to a first approximation. The theoretical predictions can be improved if the model parameters are considered as effective ones and are determined for conditions close to the experiment.

An important attribute of the metal contact zone is the pore space that is not filled with solid material. To characterize it, a standard void volume parameter is introduced,<sup>[36]</sup> which should be reflected in the model. With the continuum approach, the presence of voids in the material will be accounted for by models devised for powders and porous bodies. To that end, the porosity parameter  $\theta$  is introduced, which is defined as the volume of voids per unit volume of material. According to the stereological relations,<sup>[37]</sup> in the case of isotropy, the value of  $\theta$  is equal to the specific empty area: the area of empty regions per unit area in a cross section of the material. It follows that in the TBody model, the value  $(1 - \theta)$  corresponds to the specific area of actual contact of the rough surfaces.

Porosity is one of the internal variables. In the continuum approach, the internal variables are descriptors of the inner structure of the material. Their evolution represents the processes of its restructuring.<sup>[38]</sup> In general, internal variables depend on the deformation history of the material. Specifically, the processes leading to the formation and degradation of a cold-welded composite structure should also be reflected in the TBody model in terms of the evolution of the corresponding internal variables.

The principles of building a continuum model of powder materials and some examples of such models are known.<sup>[39–41]</sup> Many of them are based on the plasticity condition

$$f(\sigma_{ij}, \xi^k) = 0 \quad (1)$$

and the associated flow rule

$$\dot{\epsilon}_{ij} = \lambda \frac{\partial f}{\partial \sigma_{ij}} \quad (2)$$

where  $f$  is the loading function,  $\lambda$  is an undefined scalar multiplier, and  $\xi^k$  is the vector of internal variables.

For isotropic materials, the loading function depends on the stress tensor invariants (as a rule, only on the first two). In this case, the plasticity condition (1) has the form

$$f(\sigma, \tau; \xi^k) = 0 \quad (3)$$

with  $\sigma = \frac{1}{3}\sigma_{ij}\delta_{ij}$ ,  $\tau = \sqrt{(\sigma_{ij} - \sigma\delta_{ij})(\sigma_{ij} - \sigma\delta_{ij})}$  and  $\delta_{ij}$  being the Kronecker symbol.

Then it follows from (2)

$$\dot{\epsilon} = \lambda \frac{\partial f}{\partial \sigma} \quad (4)$$

$$\dot{\gamma} = \lambda \frac{\partial f}{\partial \tau} \quad (5)$$

$$\text{with } \dot{\epsilon} = \dot{\epsilon}_{ij} \delta_{ij}, \dot{\gamma} = \sqrt{(\dot{\epsilon}_{ij} - \frac{1}{3} \dot{\epsilon} \delta_{ij})(\dot{\epsilon}_{ij} - \frac{1}{3} \dot{\epsilon} \delta_{ij})}.$$

The closed curve (3) on the plane  $(\sigma, \tau)$  represents the yield locus of the powder body, and relations (4) and (5) show that the strain rate vector  $(\dot{\epsilon}, \dot{\gamma})$  is orthogonal to it.

The yield locus limits a certain convex region  $\Omega$  on the plane  $(\sigma, \tau)$ . All points mapping the stressed state of the powder body belong to  $\Omega$ , where  $f < 0$ , and its boundary, where  $f = 0$ . Outside the region  $\Omega$ ,  $f > 0$ .

Considering the relation

$$\dot{\epsilon} = \dot{\theta} / (1 - \theta) \quad (6)$$

between the rate of variation of porosity  $\dot{\theta}$  and the rate of the volume variation  $\dot{\epsilon}$  and using Equation (4) we arrive the kinetic equation for porosity

$$\frac{\dot{\theta}}{1 - \theta} = \lambda \frac{\partial f}{\partial \sigma} \quad (7)$$

The complete set of TBody equations includes, along with the constitutive equations, a set of equations of motion, the heat conduction equation, and the kinetic equations for the internal variables. To solve this set of equations, the sticking conditions and the continuity conditions for normal and tangential stresses are specified at the boundaries of the TBody.

### 3. Constitutive Equations for the TBody and Their Analysis

In this section, the constitutive relations for the TBody in a cold welding (CW) model are proposed and analyzed, based on the loading function,<sup>[42]</sup> which has already been used in TBody modeling contact friction in metal forming,<sup>[28]</sup> as well as in the studies of deformation and fracture of solids and an analysis of powder shearing under pressure.<sup>[43–45]</sup> The main difference of the model outlined below from the mentioned studies is that it accounts for the dependence of its parameters on the deformation history of the material.<sup>[28,42–45]</sup> It is this crucial feature that enables a description of the onset of deformation-induced joining and the evolution of the properties of the weld joint. The loading function of a powder body has the form<sup>[42]</sup>

$$f = \frac{\sigma^2}{\psi(\theta)} + \frac{\tau^2}{\varphi(\theta)} - (1 - \theta)k^2(\sigma) \quad (8)$$

where  $\psi(\theta)$  and  $\varphi(\theta)$  are monotonic functions of the relative porosity  $\theta$  entering the plasticity conditions for porous or powder bodies,<sup>[36–38]</sup> which satisfy the limit relations

$$\lim_{\theta \rightarrow 0} \psi(\theta) \rightarrow \infty, \quad \lim_{\theta \rightarrow 0} \varphi(\theta) \rightarrow 1 \quad (9)$$

$$k(\sigma) = \sqrt{2}K(\sigma) \quad (10)$$

where  $K(\sigma)$  is the shear yield stress of the compact powder body (figuratively, its “skeleton”).

At  $\theta = 0$ , the plasticity condition (3) corresponding to the loading function (9) is reduced to the generalized von Mises plasticity condition<sup>[32]</sup>

$$\sigma_u = \sqrt{3}K(\sigma) \quad (11)$$

$$\text{where } \sigma_u = \sqrt{3/2} \sqrt{(\sigma_{ij} - \sigma \delta_{ij})(\sigma_{ij} - \sigma \delta_{ij})} = \sqrt{3/2} \tau.$$

For the functions  $\psi(\theta)$  and  $\varphi(\theta)$ , the theoretical relations have been widely adopted<sup>[46]</sup>

$$\psi(\theta) = \frac{2(1 - \theta)^3}{3 - \theta}, \quad \varphi(\theta) = (1 - \theta)^2 \quad (12)$$

along with the formulas

$$\psi(\theta) = \frac{(1 - \theta)^{2n-1}}{6a\theta^m}, \quad \varphi(\theta) = (1 - \theta)^{2n-1} \quad (13)$$

with parameters  $a, m, n$  to be determined experimentally.<sup>[47]</sup>

The dependence  $k(\sigma)$  was presented in the piecewise-linear form<sup>[42]</sup>

$$k(\sigma) = \begin{cases} k_0 - \alpha\sigma, & \text{at } 0 \leq k_0 - \alpha\sigma \leq k_1 \\ k_1, & \text{at } k_0 - \alpha\sigma > k_1 \end{cases} \quad (14)$$

where  $k_0$  and  $k_1$  denote the adhesion coefficients and  $\alpha$  is the coefficient of friction of the individual material.

From Equation (10) it follows that, with the accuracy of a constant coefficient, the quantity  $k_0$  represents the shear yield stress of the compact powder body at zero pressure, and  $k_1$  is the limit value of this characteristic at high pressure.

The yield loci of the compact powder body for the loading functions given by Equation (8) and (14) are depicted in **Figure 2**, where dimensionless coordinates (all stresses being normalized by  $k_1$ ) are used. These yield loci satisfy the equation

$$\frac{\sigma^2}{\psi(\theta)} + \frac{\tau^2}{\varphi(\theta)} = (1 - \theta)k^2(\sigma) \quad (15)$$

Yield loci offer the possibility to obtain some useful results in a clear visual way and without calculations, cf., e.g.<sup>[35,39]</sup> In particular, irreversible deformation of the material stems only from the

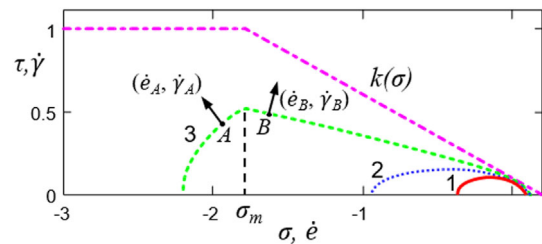


**Figure 2.** Yield loci of a compact powder body with the loading function defined by Equation (8) and (14). In the calculation it was assumed that i) the functions  $\psi(\theta)$  and  $\varphi(\theta)$  are defined by formulas (12); The following parameter values were used:  $k_0 = 0.1, k_1 = 1, \alpha = 0.5, \theta_1 = 0.20, \theta_2 = 0.15, \theta_3 = 0.10$ . The arrows on the yield locus 3 show the directions of the strain rate vector  $(\dot{\epsilon}, \dot{\gamma})$  at points A and B.

stress states, which in the  $(\sigma, \tau)$  coordinates are mapped on the points located on the yield locus. Those stress states that are mapped on the points located inside a yield locus give rise to elastic deformation only. The deformed state of the materials is represented by the plastic strain rate vector. Its origin corresponds to the point corresponding to the stress state, and its components are given by  $(\dot{\epsilon}, \dot{\gamma})$ . To that end, a coordinate system  $(\hat{\epsilon}, \hat{\gamma})$  is introduced whose axes are aligned with those of the coordinate system  $(\sigma, \tau)$ . As no plastic deformation occurs within the region confined by the yield locus, plastic deformation rate vectors associated with it are zero. Nonzero vectors  $(\hat{\epsilon}, \hat{\gamma})$  correspond only to stress states on the yield locus. If the projection of such a vector on the horizontal axis is positive, the material's porosity is increased upon straining, while in the opposite case it is decreased.

As noted in the previous section, the strain rate vector  $(\dot{\epsilon}, \dot{\gamma})$  is orthogonal to the yield locus. This implies fundamentally different behavior of the TBody in the areas of the yield locus located to the left and to the right of its maximum point  $\sigma_m$ . Indeed, while at point A located to the left of  $\sigma_m$ , the projection on the abscissa is  $\dot{\epsilon} < 0$  and the porosity of the TBody decreases with deformation, at point B located to the right of  $\sigma_m$ , one has  $\dot{\epsilon} > 0$  and the porosity of the TBody increases (see Figure 2). Thus, at pressures higher than  $-\sigma_m$ , the bonding of the metals during CW is enhanced and at pressures lower than  $-\sigma_m$  it degrades.

In what follows, we shall refer to yield locus as the limit surface of the TBody, thereby emphasizing that it limits the region  $\Omega$  on the  $(\sigma, \tau)$  plane to which the points representing the stress states of this body are mapped. The limit surface of the TBody is a comprehensive characteristic of the bond; it combines the indicators of its strength, both under tension and shear, and under combined loading in a condensed form.

Let us elucidate some properties of limit surfaces.

Figure 2 shows that the yield locus expands with a decrease in  $\theta$ . This represents strain hardening of the Tbody caused by a decrease of its porosity. Indeed, the stress states located on the yield locus for large  $\theta$ , which gave rise to irreversible deformation of the material, turn out to be located within the yield locus when  $\theta$  drops, so that no irreversible deformation occurs.

As discussed earlier, in the region  $\Omega$ , the inequality  $f < 0$  holds. Given Equation (8), it follows

$$G(\sigma, \theta) = (1 - \theta)k^2(\sigma) - \frac{\sigma^2}{\psi(\theta)} > \frac{\tau^2}{\varphi(\theta)} \geq 0 \quad (16)$$

Differentiating  $G$  with respect to  $\theta$ , one obtains

$$\frac{\partial G}{\partial \theta} = -k^2(\sigma) + \frac{\sigma^2}{(\psi(\theta))^2} \frac{d\psi}{d\theta} \quad (17)$$

With  $\frac{d\psi}{d\theta} < 0$  (see condition (9)), one has  $\frac{\partial G}{\partial \theta} < 0$  meaning that  $G$  is a decreasing function of  $\theta$ . It follows that in order to fulfil condition (16), the porosity of the TBody must satisfy the inequality

$$\theta < \theta^*(\sigma) \quad (18)$$

where  $\theta^*$  is the solution of the equation

$$(1 - \theta^*)k^2(\sigma) - \frac{\sigma^2}{\psi(\theta^*)} = 0 \quad (19)$$

With these considerations in mind, the meaning of condition (18) is that for a given hydrostatic stress  $\sigma$ , the limit surface of the TBody must circumscribe the yield locus corresponding to the porosity  $\theta^*(\sigma)$ .

There is a certain corollary regarding the initial condition for porosity,  $\theta_0$ , in the TBody problem, which follows from this requirement. Let  $\theta_{00}$  be the initial porosity of the contact zone, which it had before pressure was applied. If  $\theta_{00} > \theta^*(\sigma)$ , then according to condition (18), pressure will reduce porosity down to the value  $\theta^*(\sigma)$ . Physically, this occurs due to flattening of asperities on rough surfaces under the normal stresses only. The subsequent shear leads to a further decrease in  $\theta_{00}$ . The physical reason for that is a decrease in the load-bearing capacity of the asperities when shear stresses are applied.<sup>[35]</sup> In the TBody model, this corresponds to a transition to the overall limit surface, with a smaller value of  $\theta$ . The above considerations allow us to set the following initial conditions for porosity

$$\theta_0 = \begin{cases} \theta_{00}, & \theta_{00} < \theta^*(\sigma) \\ \kappa\theta^*(\sigma), & \theta_{00} \geq \theta^*(\sigma) \end{cases} \quad (20)$$

where  $\kappa < 1$  accounts for a decrease in porosity at the onset of shear. Below we examine the influence of this coefficient on the solution of the problem.

Let us find out the physical meaning of the parameter  $\alpha$ . To that end, we set  $k(\sigma) = k_0 - \alpha\sigma$ . After substituting expression (8) for the loading function into relations (4) and (5) and eliminating  $\lambda$ , we obtain

$$\frac{\dot{\epsilon}\tau}{\varphi(\theta)} = \dot{\gamma} \left( \frac{\sigma}{\psi(\theta)} + \alpha(1 - \theta)(k_0 - \alpha\sigma) \right) \quad (21)$$

Now, making use of Equation (9), we obtain from Equation (15) for  $\theta = 0$

$$\dot{\theta} = \alpha\dot{\gamma} \quad (22)$$

The latter relation shows that in the initially void-free bulk, porosity would be generated at a rate of  $\alpha\dot{\gamma}$ . In the context of the model, this corresponds to a mismatch between the constituent metals in the structure, which do not fully adjust to each other during plastic co-deformation. As a result, voids between them emerge. Thus, the parameter  $\alpha$  characterizes the ability of the elements of a composite structure to mutually accommodate each other during plastic deformation: the lower its value, the more effective the accommodation mechanisms are.<sup>[43]</sup>

Analysis of experiments shows that there are several critical values of pressure: a new deformation mechanism is activated each time one of them is exceeded. This gives rise to a decrease of  $\alpha$  with increasing pressure, while in the intervals between critical pressures  $\alpha$  remains constant.<sup>[42,44]</sup> Schematically, this behavior reflects the dependence expressed by Equation (14), which shows that for  $\sigma < -(k_1 - k_0)/\alpha$ , the coefficient  $\alpha$  vanishes, meaning that at a sufficiently high pressure, the structural constituents completely accommodate each other in the process of plastic deformation.

The above brief analysis shows that the parameters  $k_0, k_1$ , and  $\alpha$  are internal variables of the TBody integrally characterizing its structure. Together with the porosity  $\theta$ , they completely determine the limit surface of the TBody. The evolution of the TBody structure is reflected in the internal variable value: when a CW bond is formed,  $k_0$  increases to the level of  $k_1$ , while the value of  $\alpha$  drops since the strengthening of the metallic bond between the elements of the structure raises their adhesion to each other and promotes the accommodation mechanisms. We consider both of these factors the model proposed.

Let us take  $k_0$  the form

$$k_0 = k_1 \omega \quad (23)$$

where  $\omega \in [0, 1]$ .

The magnitude of  $\omega$  depends on the shear strain intensity, which is calculated using the formula<sup>[48]</sup>

$$\Gamma = \sqrt{2} \int_0^t \dot{\gamma} dt \quad (24)$$

as well as on the pressure, which can also change during deformation. Therefore,  $\omega$  is a functional of the deformation history in coordinates  $(\sigma, \Gamma)$ .

Let us express  $\omega$  in differential form

$$d\omega = C(\Gamma, \sigma) d\Gamma \quad (25)$$

where  $C(\Gamma, \sigma)$  is some function of shear strain intensity and hydrostatic stress.

According to experiment, the strain dependence of  $k_0$  has the form of an S-shaped curve, which can be taken into account by presenting  $C(\Gamma, \sigma)$  as a rectangular impulse function<sup>[49,50]</sup>

$$C(\Gamma, \sigma) = \begin{cases} 0, & \text{at } 0 \leq \Gamma < \Gamma_1(\sigma) \\ \beta(\sigma), & \text{at } \Gamma_1(\sigma) \leq \Gamma < \Gamma_2(\sigma) \\ 0, & \text{at } \Gamma_2(\sigma) \leq \Gamma \end{cases} \quad (26)$$

where  $\Gamma_1(\sigma)$  and  $\Gamma_2(\sigma)$  are the boundaries of the beginning and end of transformations in the TBody that change the magnitude of  $\omega$ . These functions decrease with increasing pressure.<sup>[50]</sup> Integration of (25) taking into account (26), with  $\sigma = const$ , yields

$$\omega(\Gamma, \sigma) - \omega(0, \sigma) = \begin{cases} 0, & \text{at } 0 \leq \Gamma < \Gamma_1(\sigma) \\ \beta(\sigma)\Gamma, & \text{at } \Gamma_1(\sigma) \leq \Gamma < \Gamma_2(\sigma) \\ \beta(\sigma)(\Gamma_2(\sigma) - \Gamma_1(\sigma)), & \text{at } \Gamma_2(\sigma) \leq \Gamma \end{cases} \quad (27)$$

We set the value for  $k_0$  at  $\Gamma = 0$  as  $k_0 = k_{00}$  and arrive at the equation

$$\omega(0, \sigma) = k_{00}/k_1 \quad (28)$$

Since the maximum value of  $\omega(\Gamma, \sigma)$  is equal to 1, we obtain from Equation (27)

$$\beta(\sigma) = \frac{1 - k_{00}/k_1}{\Gamma_2(\sigma) - \Gamma_1(\sigma)} \quad (29)$$

Thus, differential Equation (25), combined with the initial condition (28) and relations (23), (26), and (29), accounts for the evolution of the internal variable  $k_0$  during CW. After determining the parameters  $k_{00}, k_1$  and the functions  $\Gamma_1(\sigma), \Gamma_2(\sigma)$  in designated experiments, the above relations make it possible to find  $k_0$  in coordinates  $(\sigma, \Gamma)$  for any deformation history.

Let us show that indirectly, these relations also account for improved accommodation of the constituent structural elements when their bond is strengthened. To do this, we represent  $k(\sigma)$  in the following form, equivalent to Equation (14)

$$k(\sigma) = k_0 - \alpha^* \sigma \quad (30)$$

where the coefficient  $\alpha^*$  is given by

$$\alpha^* = \alpha H(\sigma + (k_1 - k_0)/\alpha) \quad (31)$$

Here  $H(\xi) = \begin{cases} 0, & \xi < 0 \\ 1, & \xi \geq 0 \end{cases}$  is the Heaviside function.

In relation (30), instead of the internal variable  $\alpha$ , which is responsible for the accommodation of the TBody structure as expressed by Equation (14), the parameter  $\alpha^*$  appears. Equation (31) shows that with increasing  $k_0$ , the pressure range with  $\alpha^* = 0$  expands. This means improved accommodation of the structural elements of the TBody.

For convenience of subsequent analysis of the model and use of its results, we now write down the constitutive equations of TBody in their final form.

From (21) and (25) we have

$$\frac{d\theta}{d\Gamma} = \frac{\varphi(\theta)(1 - \theta)}{\sqrt{2}\tau} \left( \frac{\sigma}{\psi(\theta)} + \alpha(1 - \theta)k(\Gamma, \sigma) \right) \quad (32)$$

$$\frac{d\omega}{d\Gamma} = C(\Gamma, \sigma) \quad (33)$$

where

$$C(\Gamma, \sigma) = \begin{cases} 0, & \text{at } 0 \leq \Gamma < \Gamma_1(\sigma) \\ \frac{1 - k_{00}/k_1}{\Gamma_2(\sigma) - \Gamma_1(\sigma)}, & \text{at } \Gamma_1(\sigma) \leq \Gamma < \Gamma_2(\sigma) \\ 0, & \text{at } \Gamma_2(\sigma) \leq \Gamma \end{cases} \quad (34)$$

$$\tau = \sqrt{\varphi(\theta)G(\sigma, \Gamma, \theta)} \quad (35)$$

$$G(\sigma, \Gamma, \theta) = (1 - \theta)k^2(\sigma, \Gamma) - \frac{\sigma^2}{\psi(\theta)} \quad (36)$$

$$k(\sigma, \Gamma) = k_1 \omega - \alpha \sigma H(\sigma + k_1(1 - \omega)/\alpha) \quad (37)$$

The initial conditions (20) and (28) read for  $\Gamma = 0$

$$\omega_0 = k_{00}/k_1, \theta_0 = \begin{cases} \theta_{00}, & \theta_{00} < \theta^*(\sigma) \\ \kappa \theta^*(\sigma), & \theta_{00} \geq \theta^*(\sigma) \end{cases} \quad (38)$$

where  $\theta^*(\sigma)$  is the solution of the equation  $G(\sigma, \theta^*) = 0$  for  $\kappa < 1$ .

Equation (32)–(38) describe the behavior of the TBody and the concomitant evolution of the properties of a CW bond. They are to be solved using the coupled problem approach to metal forming, together with the pertinent equations for the co-deforming metals comprising the pair to be joined. At the same time, at the

boundaries between the TBody and the metals of the pair the requirement of continuity of the velocity field, as well as the normal and tangential stresses must be imposed.

The problem is significantly simplified if the deformation history  $\sigma(\Gamma)$  is known. In this case, Equation (33) can be solved independently of (32), which enables finding  $\omega(\Gamma)$ . Substituting this function into (32) and determining  $\theta(\Gamma)$  completely solves the problem of calculating the limit surface for a given deformation history of the TBody.

Figure 3a shows the limit surfaces for TBody constructed according to Equation (15) with the values of  $\theta$  and  $\omega$  obtained by solving Equation (32)–(38) for six deformation histories shown in Figure 3b. The calculations were performed under the following conditions: the functions  $\psi(\theta)$  and  $\varphi(\theta)$  were defined by Equation (12) with  $k_1 = 1$  (all stresses being normalized with respect to  $k_1$ ),  $k_{0,0} = 0.1$ ,  $\alpha = 0.3$ ; the critical (threshold) strains  $\Gamma_1(\sigma)$  and  $\Gamma_2(\sigma)$  are given by the formulas  $\Gamma_1(\sigma) = -20/\sigma$  and  $\Gamma_2(\sigma) = -40/\sigma$ ;  $\kappa$  was set at 0.9.

To conclude this section, we compare our proposed TBody approach with the film theory (FT),<sup>[49]</sup> which serves as a basis for current models of CW that describe joining of metals by plastic deformation under pressure.<sup>[16]</sup> In outline, FT entails the following concepts: 1) gripping of metals in contact with each other is hindered by a surface film; 2) under co-deformation of the

metals the contact area is increased leading to destruction of the film; and 3) under the action of a sufficiently high contact pressure the metals, now unprotected by a film, are extruded into gaps between the metals and come into immediate contact, which leads to the formation of a strong junction. This approach is effective for CW processes, which involve elongation (rolling, stamping) when the nominal contact area is increased.<sup>[16]</sup> Under simple shear, the nominal contact area is practically unchanged, so that FT cannot be applied. In that case, the disruption of isolating surface films is associated with an increase of the actual contact area resulting from rotations caused by simple shear.<sup>[13–15]</sup> The phenomenological TBody approach captures this effect in terms of the  $\omega$  function expressed by the kinetic Equation (25). This equation relates the variation of  $\omega$  to the increment of the shear strain. The said equation can be complemented by including an additive term on the right-hand side to account for the variation of  $\omega$  due to the increase of the nominal contact area induced by the elongation strain. Such a generalized formulation would provide the model with the capacity to describe CW effected by any deformation processes.

#### 4. Experimental Approach and Methodology for Identifying Model Parameters

Experimental investigations on the welding of samples through shear deformation under pressure were carried out at the Institute for Metal Forming Technology (IFU) at the University of Stuttgart. The thermomechanical testing machine utilized for these experiments was the Gleeble 3800 C, equipped with a torsion module capable of both rotational and axial movements. Load cells for torque and axial load measurement, along with scales for rotation angle and stroke measurement, were integrated into the machine for precise process control. Movement profiles were defined by configuring axial and rotational displacement or load and torque limits, allowing for the combination of both axial and rotational movement.

For this study, aluminum 6060 in a soft annealed state (380 °C, 1.5 h) served as the material for the specimens. Cylindrical samples with a diameter of 10 mm and a length of 15 mm, featuring a contoured face as illustrated in Figure 4a with a ring-shaped contact area, were employed. A tapered portion on the outer ring supported the contact layer, and a central hole in the specimen ( $\varnothing 3.5$  mm and a depth of 1 mm) eliminated areas

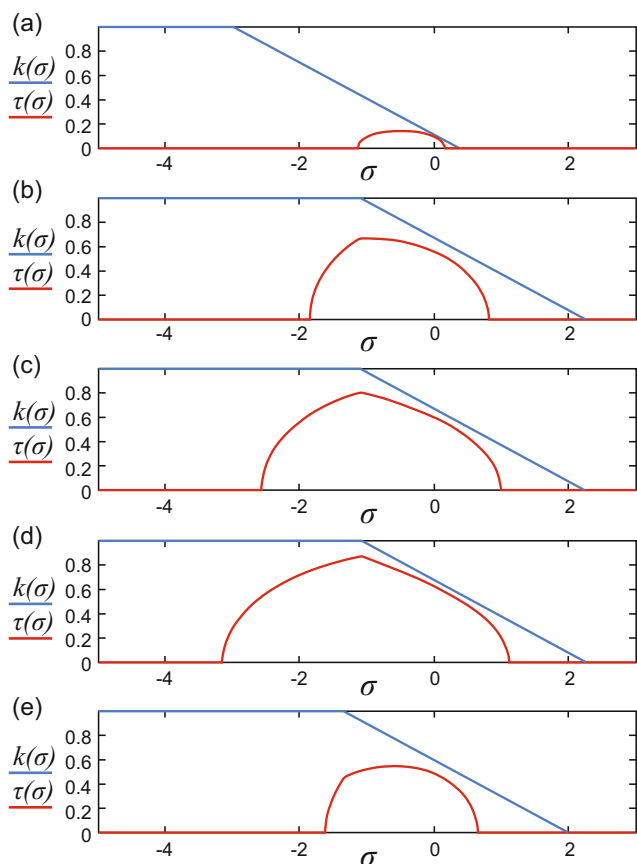


**Figure 3.** TBody limit surfaces for five deformation histories: a)  $\sigma = -0.5$ , b)  $\sigma = -1$ , c)  $\sigma = -2$ , d)  $\sigma = -3$ , e)  $\sigma = -1$  when  $0 \leq \Gamma < 20$ ,  $\sigma$  decreases linearly from  $(-1)$  to  $(-3)$  when  $20 \leq \Gamma \leq 40$ .

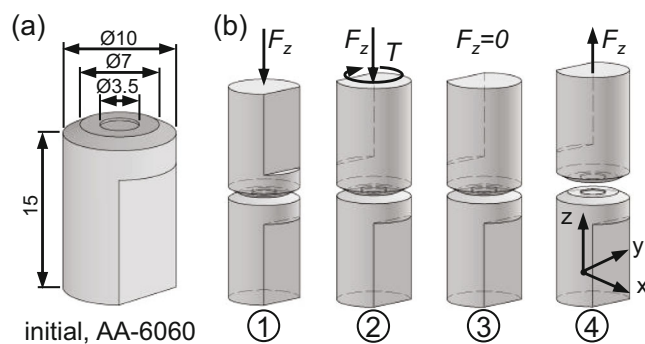


**Figure 4.** Experimental scheme: a) sample design; b) loading stages.

of low deformation. The experiments were conducted at room temperature.

Figure 4b illustrates the four stages of the experiment. In the initial stage, the samples were compressed with a specified force—here, 1000 N, corresponding to one-third of the yield strength. During the second stage, one of the samples underwent rotation at an angular velocity of 1 rpm until reaching a rotation angle of 90 degrees, while the compressive force was automatically maintained at the designated level. The third stage involved the removal of the compressive load, while residual stresses, expressed in the form of torque, persisted. Finally, in the fourth stage, the welded joint was subjected to tensile test until failure.

Figure 5 presents the outcomes of shear welding under pressure. In Figure 5a, the visual depiction of the contact surfaces of the samples is showcased. Upon a straightforward visual examination of the surfaces post-joint failure, it becomes evident that the contact area remains virtually unaltered. However, a notable observation is the presence of numerous microvortices on the surface, a phenomenon consistently noted in previous instances of shearing multilayer samples under pressure.<sup>[51,52]</sup>

Figure 5b illustrates a noteworthy increase in the force moment during the second stage of the experiment, signaling the strengthening of the TBody attributed to the formation of a metallic compound. At the point when the rotation ceased (25 s), the compression force applied to the samples was  $F_1 = -1000$  N, and the torsional torque was  $T_1 = 6.64$  Nm. Correspondingly, the calculated stresses in the connection zone (third body), using established relationships for the sample dimensions depicted in Figure 4a, were normal stress  $\sigma_n = -34.6$  MPa and tangential stress  $\tau_t = 84.5$  MPa. Upon subsequent stretching, the connection failed at a force of  $F_2 = 330$  N, corresponding to a stress  $\sigma_n = 11.4$  MPa, and a torsional moment of  $T_2 = 4.15$  Nm, corresponding to a tangential stress  $\tau_t = 52.8$  MPa. These values represent the stresses

averaged over a ring-shaped area of contact between the upper and the lower specimens (inner diameter 3.5 mm and outer diameter 7 mm), see Figure 4a.

For the evaluation of the characteristics of the TBody, we assume  $\theta = 0$  as a first approximation. The relationship between  $\tau$  and  $\sigma$  according to the model is taken in the form

$$\tau = k_0 - \alpha\sigma \quad (39)$$

Let us formulate this relationship for both instances—when the rotation stops and when the connection breaks. Utilizing the relationships  $\tau = \sqrt{2/3} \sigma_u = \sqrt{2/3} \cdot \sqrt{\sigma_n^2 + 3(\tau_t)^2}$ ,  $\sigma = \sigma_n/3$ , valid for uniaxial loading with shear, and incorporating the stress values derived earlier, a system of two equations emerges for determining the parameters  $k_0$  and  $\alpha$ . The obtained results are  $k_0 = 87.1$  MPa,  $\alpha = 3.09$ .

This example underscores the significant impact of the parameter  $\alpha$ , emphasizing its correlation with a powder material containing solid particles rather than an aluminum alloy.<sup>[42,42]</sup> As indicated by relation (32), this results in a rapid increase in the porosity of the TBody during tension, contributing to a comparatively lower tensile strength of the joint when compared with the inherent strength of the alloy.

The elevated value of  $\alpha$  is physically attributed to the presence of solid inclusions within the material's structure that exhibits poor accommodation during deformation. In the TBody, these inclusions may manifest as metal fragments reinforced by dispersed oxides, originally situated on the surface of the welded samples. Further exploration and discussion of this phenomenon promise to be of significant interest, with subsequent works delving into experimental studies on the composition and structure of the compound. They will be focused on discovering the optimal ways and parameters of metal bonding leading to a low  $\alpha$  coefficient, similar to that of the original materials, which will guarantee the integrity and reliability of the bond.

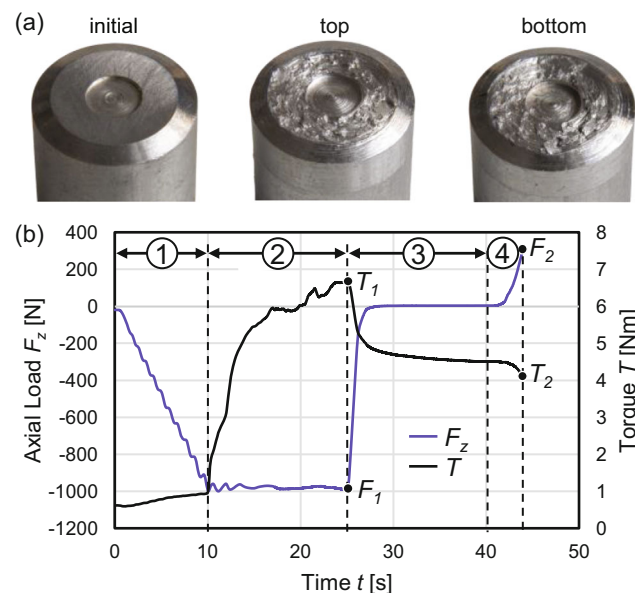


**Figure 5.** The results of the experiment: a) photographs of the samples before and after the connection was broken; b) plots of the applied force and torsional moment versus time.

## 5. Conclusion

The article introduces a novel approach to elucidating the process of CW between two metals subjected to simple shear under pressure. This method hinges on the concept of a “third body,” formed by the surfaces and subsurface zones of the two metals involved in the connection. By adopting this perspective, the intricate mathematical modeling of the welding process is streamlined into investigating the limit state of the “third body” under complex loading conditions. Consequently, the calculation of the strength of the joint is simplified, in that it is replaced by the determination of the limiting stresses for the “third body.”

Furthermore, the article proposes rheological relationships for the “third body,” drawing inspiration from a model featuring a porous material with a structurally inhomogeneous frame. This model is demonstrated to accurately capture the joint's properties, accounting for the impact of its formation history on weld strength. The rheological relationships for the “third body” incorporate two fitting parameters: the first representing the shear stress of the frame and the second reflecting the structural elements' capacity to adjust during joint deformation.

The experimental methodology for shear welding under pressure is detailed in the article, along with preliminary results. This practical illustration serves to elucidate the process of determining the fitting parameters of the proposed model and provides insightful interpretations within the model's framework.

We have shown that the concept of a “third body”—a layer between two contacting metals formed during shear deformation—is a useful modeling tool to describe the formation of a bond between the metals. It enables a mathematical description of the deformation of the bond along with the deformation of the metals forming the joint, as well as its evolution during subsequent plastic deformation of the resulting composite material.

## Acknowledgements

Y.B., Y.E., and R.K. acknowledge support from The Volkswagen Foundation through the Project Az.: 97751.

Open Access funding enabled and organized by Projekt DEAL.

## Conflict of Interest

The authors declare no conflict of interest.

## Data Availability Statement

The data that support the findings of this study are available from the corresponding author upon reasonable request.

## Keywords

cold welding, composite materials, simple shear, third body

Received: February 14, 2024

Revised: March 31, 2024

Published online:

- [1] V. M. Segal, *Materials* **2018**, *11*, 1175.
- [2] Y. Beygelzimer, L. S. Toth, J. J. Jonas, *Adv. Eng. Mater.* **2015**, *17*, 1783.
- [3] V. M. Segal, *Mater. Sci. Eng. A* **2002**, *338*, 331.
- [4] Y. Beygelzimer, Ruslan Z. Valiev, V. Varyukhin, *Mater. Sci. Forum* **2011**, *667–669*, 97.
- [5] P. W. Bridgman, *Phys. Rev.* **1935**, *48*, 825.
- [6] A. P. Zhilyaev, T. G. Langdon, *Prog. Mater. Sci.* **2008**, *53*, 893.
- [7] A. Bachmaier, R. Pippan, *Mater. Trans.* **2019**, *60*, 1256.
- [8] R. Z. Valiev, T. G. Langdon, *Prog. Mater. Sci.* **2006**, *51*, 881.
- [9] V. Varyukhin, Y. Beygelzimer, R. Kulagin, O. Prokof'eva, A. Reshetov, *Mater. Sci. Forum* **2010**, *667–669*, 31.
- [10] K. Edalati, A. Bachmaier, V. A. Beloshenko, Y. Beygelzimer, V. D. Blank, W. J. Botta, K. Bryła, J. Čížek, S. Divinski, N. A. Enikeev, Y. Estrin, G. Faraji, R. B. Figueiredo, M. Fuji, T. Furuta, T. Grosdidier, J. Gubicza, A. Hohenwarter, Z. Horita, J. Huot, Y. Ikoma, M. Janeček, M. Kawasaki, P. Král, S. Kuramoto, T. G. Langdon, D. R. Leiva, V. I. Levitas, A. Mazilkin, M. Mito, et al., *Mater. Res. Lett.* **2022**, *10*, 163.
- [11] A. Bachmaier, R. Pippan, *Intern. Mater. Rev.* **2013**, *58:1*, 41.
- [12] M. Vaidya, S. Sen, X. Zhang, L. Frommeyer, L. Rogal, S. Sankaran, B. Grabowski, G. Wilde, S. V. Divinski, *Acta Mater.* **2020**, *196*, 220.
- [13] R. Kulagin, Y. Beygelzimer, Y. Ivanisenko, A. Mazilkin, H. Hahn, *Mater. Sci. Eng.* **2017**, *194*, 012045.
- [14] H.-J. Kim, S. Karthikeyan, D. Rigney, *Wear* **2009**, *267*, 1130.
- [15] D. A. Rigney, S. Karthikeyan, *Tribol. Lett.* **2010**, *39*, 3.
- [16] K. Mori, N. Bay, L. Fratini, F. Micari, A. E. Tekkaya, *CIRP Ann.* **2013**, *62*, 673.
- [17] K. Fujiwara, R. Uehiro, K. Edalati, H.-W. Li, R. Floriano, E. Akiba, Z. Horita, *Mater. Trans.* **2018**, *59*, 741.
- [18] K. Edalati, R. Uehiro, K. Fujiwara, Y. Ikeda, H.-W. Li, X. Sauvage, R. Z. Valiev, E. Akiba, I. Tanaka, Z. Horita, *Mater. Sci. Eng. A* **2017**, *701*, 158.
- [19] R. Lapovok, M. R. G. Ferdowsi, V. Shterner, P. D. Hodgson, A. Mazilkin, E. Boltynjuk, R. Kulagin, S. L. Semiatin, *Adv. Eng. Mater.* **2024**, 2301949, <https://doi.org/10.1002/adem.202400388>.
- [20] K. S. Kormout, R. Pippan, A. Bachmaier, *Adv. Eng. Mater.* **2017**, *19*, 1600675.
- [21] R. Kulagin, Y. Beygelzimer, A. Bachmaier, R. Pippan, Y. Estrin, *Appl. Mater. Today* **2019**, *15*, 236.
- [22] K. S. Kormout, B. Yang, R. Pippan, *Adv. Eng. Mater.* **2015**, *17*, 1828.
- [23] O. Renk, M. Tkadletz, N. Kostoglou, I. E. Gunduz, K. Fezzaa, T. Sun, A. Stark, C. C. Doumanidis, J. Eckert, R. Pippan, C. Mitterer, C. Rebholz, *J. Alloys Compd.* **2021**, *857*, 157503.
- [24] M. Godet, *Wear* **1990**, *136*, 29.
- [25] Y. Berthier, in *Third-Body Reality - Consequences and Use of the Third-Body Concept to Solve Friction and Wear Problems. Wear – Materials, Mechanisms and Practice*, (Ed: G. W. Stachowiak), **2014**.
- [26] K. Lontin, M. Khan, *Friction* **2021**, *9*, 1319.
- [27] I. Iordanoff, Y. Berthier, S. Descartes, H. Heshmat, *ASME. J. Tribol.* **2002**, *124*, 725.
- [28] Y. E. Beygelzimer, A. A. Milanin, V. Z. Spuskanyuk, *J. Frict. Wear* **1993**, *4*, 471.
- [29] N. Fillot, I. Iordanoff, Y. Berthier, in *Proceedings of the World Tribology Congress III*, Washington, D.C., USA **2005**.
- [30] A. Ghiotti, S. Bruschi, M. Kain, L. Lizzul, E. Simonetto, G. Tosello, *J. Manuf. Process.* **2021**, *72*, 105.
- [31] F. Pereira, N. Dourado, J. J. L. Morais, M. F. S. F. de Moura, *Eng. Fract. Mech.* **2022**, *271*, 108594.
- [32] S. C. Lim, M. F. Ashby, J. H. Brunton, *Acta Metall.* **1989**, *37*, 767.
- [33] A. Molinari, Y. Estrin, S. Mercier, *J. Tribol.* **1999**, *121*, 35.
- [34] G. Z. Voyiadjis, B. Deliktas, D. Faghihi, A. Lodygowski, *Acta Mech.* **2010**, *213*, 39.
- [35] R. Hill, *The Mathematical Theory of Plasticity*, Oxford University Press, England **1998**.
- [36] F. Blateyron, in *Characterisation of Areal Surface Texture* (Ed: R. Leach), Springer, Berlin, Heidelberg **2013**.
- [37] E. E. Underwood, in *Microstructural Analysis* (Eds: J. L. McCall, W. M. Mueller) Springer, Boston **1973**.
- [38] J. R. Rice, *J. Mech. Phys. Solids* **1971**, *19*, 433.
- [39] A. C. F. Cocks, in *Modelling of Powder Die Compaction. Engineering Materials and Processes* (Eds: P. R. Brewin, O. Coube, P. Doremus, J. H. Tweed). Springer, London **2008**.
- [40] M. Shtern, *Proc. of the IUTAM Symp.*, Springer, Dordrecht **1997**, p. 95.
- [41] M. Shtern, O. Mikhailov, A. Mikhailov, *Powder Metall. Met. Ceram.* **2021**, *60*, 20.
- [42] Y. E. Beigelzimer, A. P. Getmanskii, L. I. Alistratov, *Powder Metall. Met. Ceram.* **1986**, *25*, 952.
- [43] J. E. Beigelzimer, B. Efros, V. Varyukhin, A. Khokhlov, *Eng. Fract. Mech.* **1994**, *48*, 629.
- [44] Y. Beygelzimer, *Mech. Mater.* **2005**, *37*, 753.
- [45] R. Kulagin, Y. Zhao, Y. Beygelzimer, L. S. Toth, M. Shtern, *Mater. Res. Lett.* **2017**, *5*, 179.
- [46] E. A. Olevskii, M. B. Shtern, *Powder Metall. Met. Ceram.* **2004**, *43*, 355.
- [47] A. M. Laptev, *Powder Metall. Met. Ceram.* **1982**, *21*, 522.

- [48] L. M. Kachanov, *Fundamentals of The Theory of Plasticity*, Dover Publications Inc., Mineola, NY **2004**.
- [49] W. Zhang, N. Bay, *CIRP Annals* **1996**, 45, 215.
- [50] W. Zhang, N. Bay, T. Wanheim, *CIRP Annals* **1992**, 41, 293.
- [51] V. Tavakkoli, A. Mazilkin, T. Scherer, M. Mail, Y. Beygelzimer, B. Baretzky, Y. Estrin, R. Kulagin, *Mater. Lett.* **2021**, 302, 130378.
- [52] Y. Beygelzimer, Y. Estrin, A. Filippov, A. Mazilkin, M. Mail, B. Baretzky, R. Kulagin, *Mater. Lett.* **2022**, 324, 132689.